Trace-based and geostatistical inversion of 3-D seismic data for thin-sand delineation: An application in San Jorge Basin, Argentina

CARLOS TORRES-VERDÍN, *The University of Texas at Austin, U.S. (formerly with YPF SA)*
MARCOS VICTORIA, and GERMÁN MERLETTI, *YPF SA Buenos Aires, Argentina*
JOHN PENDREL, *Jason Geosystems, Calgary, Canada*

Argentina's San Jorge Basin, which straddles the southern provinces of Chubut and Santa Cruz in the heart of Patagonia, has been producing hydrocarbons since 1907. The region currently accounts for 32% of the country's production. The existence and early geologic evolution of the basin is due to the same rift process responsible for the opening of the Atlantic Ocean in early Jurassic times. Extensive direct faulting and local erosion accompanied the rift evolution, thereby facilitating the accumulation of chiefly nonmarine terrigenous sediments well into the early Cretaceous. At this point, Andean tectonism became a major source of pyroclastic concentration in the sedimentary column; it was also responsible for pervasive batholitic intrusions. Clastic deposition in the hydrocarbon-producing zone is characterized by thick shale laminations of lacustrine and floodplain origin, interspersed with much thinner and laterally sparse sand bodies (the hydrocarbon reservoirs).

The relatively small concentration of sand bodies in the sedimentary column is explained by their ephemeral fluvial and alluvial architectures that developed into beds with thicknesses of only 1-15 m (but predominantly thinner than 4 m). The sedimentary column was further modified by the intercalation of finely laminated deposits of pyroclastic origin (tuffs) that could often reach thicknesses of several meters. Both in-situ porosity and permeability of useful sand bodies remained conditioned by both tuffaceous component and subsequent structural deformation.

This paper describes a small portion of the basin on its southern flank, Cañadón de la Escondida. Oil-producing sands pertain to the Bajo Barreal Formation (mid and upper Cretaceous) and are buried at depths of 1200-2000 m.

Figure 1 shows approximately 450 wells in Cañadón de la Escondida that seem distributed in the form of dispersed clusters. This distribution is due to the laterally discontinuous character of reservoir sands but also reveals a well-placement methodology based on stepout front development. In the past, wells were often placed only with regard to structural play inferred from surface geology and, in some cases, 2-D seismic data, because geoscientists had few clues about the presence or lateral continuity of sands.

However, stepout front development has been uneconomic in Cañadón de la Escondida; 95% of production over the life of the field has come from just 5% of the wells. (Average production per well is 6 m^3/day and average accumulated production per well is 13 000 m^3).

In an effort to substantially improve development, we attempted to shed further light on the vertical and lateral extent of sands by using amplitude information in 3-D poststack seismic data. Standard seismic attributes are dubious indicators of sand continuity in the Cañadón de la Escondida area because of tuning effects. Therefore, prior to establishing a petrophysical relationship between sand presence and seismic response, the wavelet footprint must be eliminated from the data. We used trace-based inversion to solve this problem and then tried to increase the vertical resolution

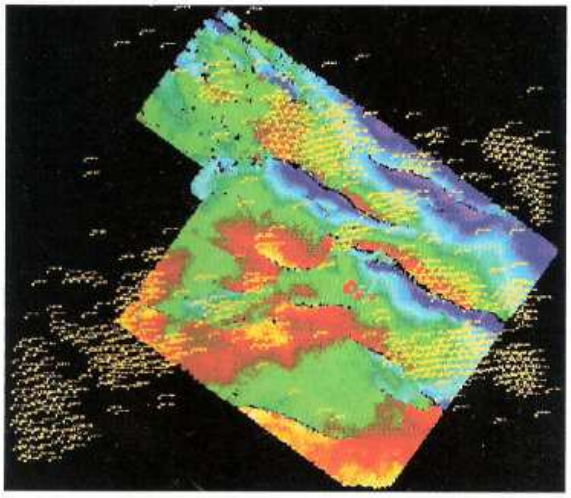

Figure 1. Base map of the Cañadón de la Escondida project describing well locations with yellow dots. A rainbow-color-coded time horizon indicates the spatial extent of the seismic data: Early times are in red and late times in purple. Dimensions of the seismic cube are 12 × 16 km.

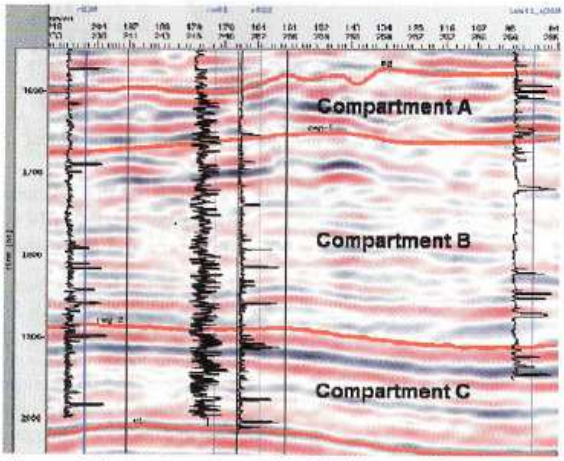

Figure 2. Seismic cross-section in time with horizons interpreted to mark the vertical boundaries of natural compaction compartments A, B, and C. Sand-fraction logs are posted at four well locations. This cross-section covers a length of approximately 7 km.

yielded by the data via a geostatistical inversion technique based on stochastic simulation. The idea was to complement the lateral resolution of the seismic data with the relatively much higher vertical resolution of wellbore data.

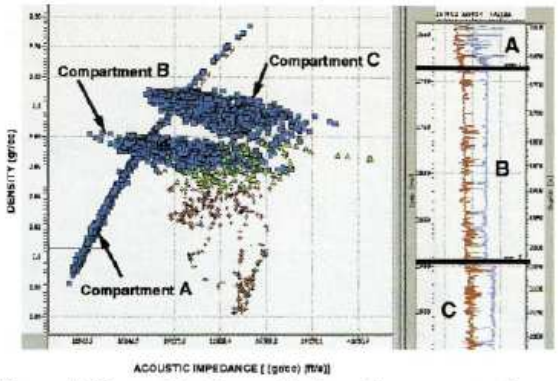

Figure 3. Crossplot of acoustic impedance versus density showing three distinct compaction trends. Blue, green, and red dots identify shales/tuffs, tight sands, and porous sands, respectively.

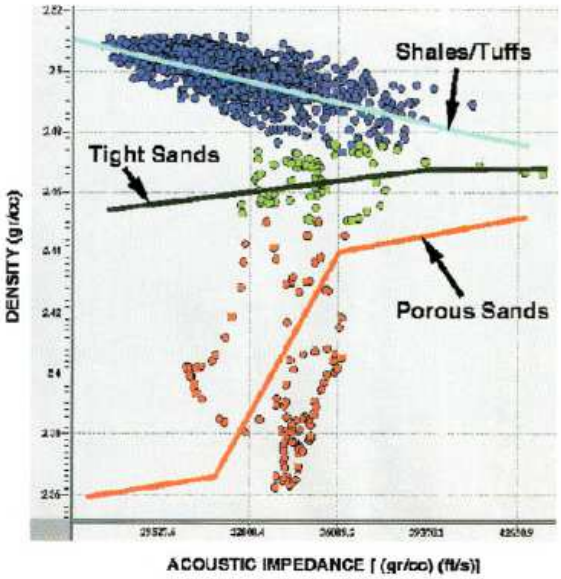

Figure 4. Crossplot of acoustic impedance versus density within compartment C. Lithology differentiation was performed using SP, resistivity, and nuclear density logs. Solid lines shown for each lithology correspond to best-fit piecewise linear trends.

Geostatistical inversion allows the information from all available measurements to be integrated into a unique, consistent image of the reservoir. The following sections describe the assumptions, procedures, and results of this novel methodology for thin-sand delineation.

The seismic data. The 3-D seismic data were sampled at 2 ms and have a frequency band of 6-85 Hz, with a central frequency of 35 Hz. At a frequency of 50 Hz, and assuming a *P*-wave velocity of 3200 m/s, the tuning wavelength ($\lambda/4$) is 12.5 m. This is about the best vertical resolution we can recover solely from the seismic data.

The 3-D survey in Cañadón de la Escondida consisted of 483 cross-lines (12 km) and 643 in-lines (16 km), evenly spaced at 25 m intervals. This generated 310 000 traces over 194 km^2. Figure 2 is a typical time-domain cross-section. The interpreted horizons delineate limits between natural vertical compartments (denoted A, B, and C) in the production

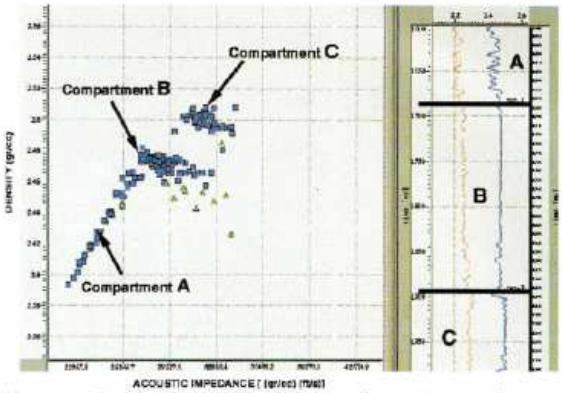

Figure 5. Crossplot of acoustic impedance versus density within the same frequency band of the seismic data.

zone. Processing and poststack time migration preserved true amplitudes and minimized the spatial aliasing inherent to the acquisition pattern.

The petrophysical data. Crossplots of *P*-wave acoustic impedance (AI) versus density derived from wellbore measurements reveal interesting compaction patterns. The plot in Figure 3 shows clear evidence of three vertical compartments. First, the parabolic and monotonically increasing branch corresponds to wellbore measurements acquired along compartment A in Figure 2. Next, the monotonically decreasing lower parabolic branch corresponds to wellbore measurements made within compartment B. Finally, the upper parabolic, monotonically decreasing branch is associated with wellbore measurements acquired along compartment C. Branch A describes typical shale compaction due

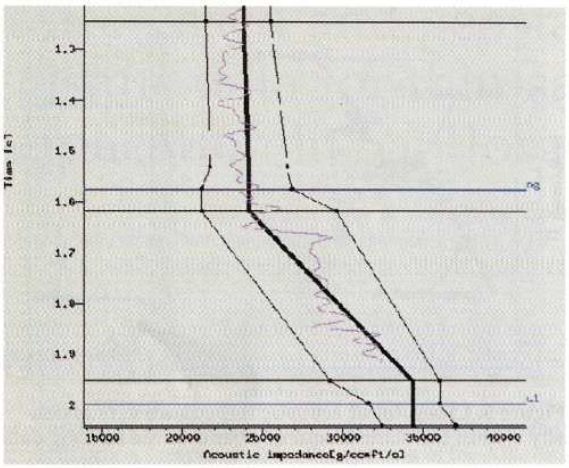

Figure 6. Example of upper and lower bound constraints enforced during the inversion of seismic data into acoustic impedances. The constraint lines, shown in thin black, enclose the mean compaction trend (in thick black), as well as acoustic impedance fluctuations exhibited by control logs (in magenta).

to hydrostatic stress. Compartments B and C, however, exhibit anomalous behavior with respect to compartment A.

Core studies imply that this anomalous behavior is due to finely laminated pyroclasts whose mechanical compaction régime dominates shales in the composite mixture. Moreover, the obvious discontinuous jump between B and C is due to the larger concentration of pyroclasts in the latter. A substantial concentration of pyroclasts in the otherwise primarily shaly sequence affects the mechanical competence of the composite. The resulting sequence is more prone to fracturing than the corresponding shaly mixture when subject to the same stress regime; this affects in-situ porosity-permeability relationships. Time horizons in Figure 2 were actually interpreted by tracking the boundaries of the three vertical compartments in Figure 3. Figure 4, a blown-up crossplot for compartment C, shows that at full log resolution lithology discrimination is nonunique with AI measurements alone. The same AI value can be derived from shales, tight sands, or porous sands. However, the plot shows that wellbore density could uniquely discriminate among the three lithologies (the lower the density, the larger the porosity). The unfortunate news is that poststack seismic data inverted to yield acoustic impedances are unable to discriminate lithology. This can be done only with an additional measurement uniquely related to AI.

Lithology uniqueness and vertical resolution. In an effort to understand the resolving capabilities of seismic data, we low-pass filtered the AI and density data to retain only frequency components below 85 Hz. Figure 5, the corresponding crossplot, retains the three compaction compartments despite the lower frequency range. Most interestingly, wellbore samples associated with sand packets (green) are now visible at the highest AI values within each compaction compartment. In other words, although the lower vertical resolution of seismic data vis-à-vis wellbore data precludes individual sand identification, it does allow sand-packet differentiation (sand-shale mixtures with predominant sand content) from shale/tuff sequences. The problem of nonunique AI response with respect to lithology at wellbore frequencies is therefore traded for unique correspondence at seismic frequencies (at the expense of vertical resolution).

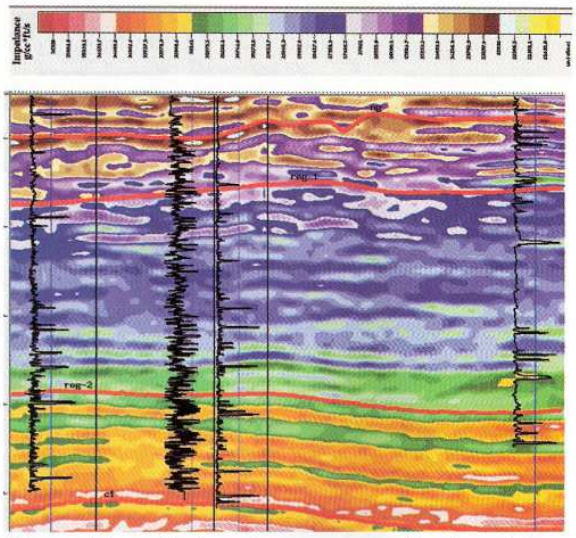

Figure 7. Acoustic impedance cross-section inverted along the same section shown in Figure 2. The color scale above describes the acoustic impedance range, with low and high values at the bottom and top, respectively.

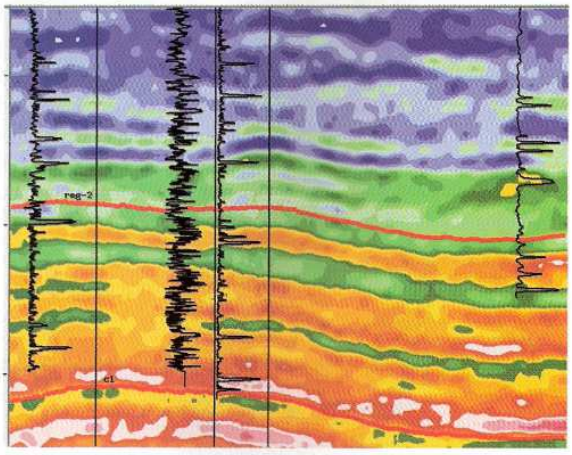

Figure 8. Close-up view of the acoustic impedance cross-section inverted along the same section shown in Figure 2. In general, high values of sand-fraction logs coincide with high values of acoustic impedance. See scale in Figure 7.

Although this has not been validated with core data, effective-medium theory calculations, or full waveform sonic logging, we have observed the same behavior in all control wells in Cañadón de la Escondida. A physical explanation could be frequency dispersion in the propagation of seismic waves through the composite media, especially when pyroclast content is significant. Acoustic impedances derived from VSP corridor stacks have shown the same behavior.

Trace-based inversion. Trace-based inversion of the 3-D seismic data was performed with a sparse-spike algorithm that enforces time-dependent bound constraints on the results. This algorithm consistently recovered features up to 70 Hz in resolution without visible noise. For wavelet estimation, we used VSP and check-shot data from 17 control wells. Sonic and density logs were edited and consistency processed (balancing) to minimize borehole rugosity effects

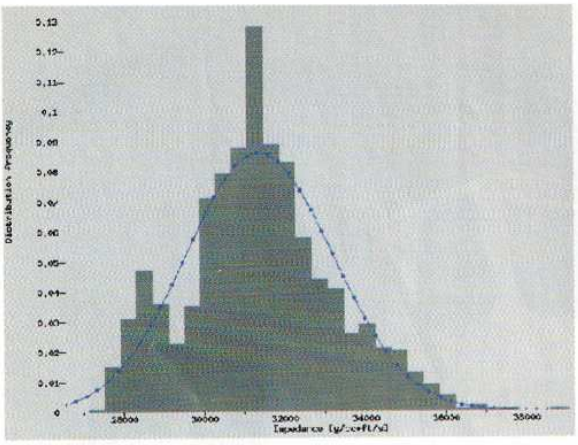

Figure 9. Example of histogram sampled from wellbore measurements of acoustic impedance. A best-fit Gaussian distribution is shown in blue for reference. The bimodal behavior in the sampled histogram is due to the influence of two main lithology types.

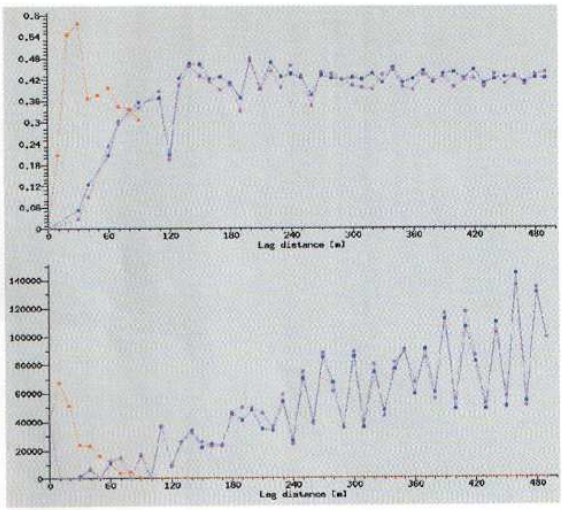

Figure 10. Example of horizontal and vertical variograms estimated from acoustic impedances. Blue, magenta, and red lines are used to identify variograms and samples estimated/acquired in the in-line, cross-line, and vertical directions, respectively. The lower panel indicates the number of samples included in the estimation of the variogram at a given lag distance.

and, hence, to reflect deep reservoir properties. Estimated wavelets were quite consistent. The bound constraints provide some stabilization in the presence of noise and narrow the space of solutions. Figure 6 shows how upper and lower bound constraints are imposed at a control well to respect the main compaction trend (solid black line) and the main excursions by the AI wellbore data (magenta). Low-frequency information not available from the seismic data but necessary to reveal the compaction trend (0-6 Hz in our case) was simulated numerically by weighted lateral interpolation of AI wellbore data from all control wells. This information was subsequently overlapped (overlap band of 6 Hz) with acoustic impedances inverted from the seismic data. Figure 7 is a cross-section of total AI (numerically simulated low-frequency AI plus inverted high-frequency AI) along the same cross-section shown in Figure 2. Extensive quality control tied wellbore acoustic impedances with those inverted from the seismic data; this QC included synthetic seismograms and an average wavelet for the whole project. In general, the match was from very good to excellent. As expected, sand packets indicated by the sand-fraction logs manifest themselves as high AI anomalies. Predominantly shaly sequences coincide with low AI values. This agrees with Figure 5 and is further emphasized by the close-up view in Figure 8.

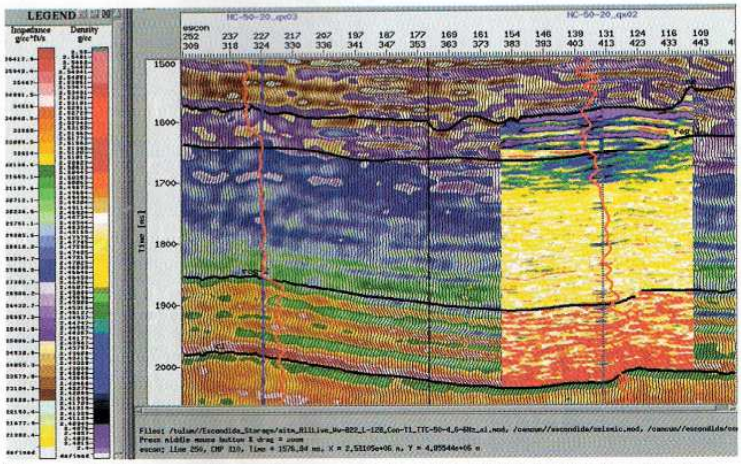

Figure 11. Cross-section of reservoir density estimated in the vicinity of a control well. Acoustic impedances obtained with trace-based inversion are displayed in the background for reference. Black wiggles are the original seismic traces. The color scales to the left describe the acoustic impedance/density range, with low and high values at the bottom and top, respectively.

Geostatistical inversion. Cañadón de la Escondida is a unique reservoir characterization project in that extensive well and geologic control complements the seismic data. In principle, the relatively high spatial sampling rate of wellbore data could improve the vertical resolution of the sand packets detected with seismic data alone. The objective would be to delineate individual sand units rather than shaly sand packets.

Haas and Dubrule, to our knowledge, made the first successful attempt to simultaneously honor seismic and wellbore data in producing geostatistical estimates of reservoir parameters between wells (although an earlier suggestion can be traced back to Journel and Huijbregts). The technique is based on random-walk stochastic simulation of acoustic impedances with an acceptance/rejection gate based on fit to the actual seismic data. This implementation considerably narrows the space of solutions and is less dependent on variogram behavior than standard geostatistical estimation. We used a similar estimation technique, in which, in addition to inverting for AI values, a stochastic cosimulation yields independent realizations of lithology and density. These random realizations satisfy probability density functions (PDFs) estimated and adjusted from sample histograms of wellbore data. Both realizations are made to satisfy a local correlation length dictated by their corresponding variograms. In the vertical direction, variograms are estimated from wellbore measurements, and in the horizontal direction variograms are estimated from AI values derived

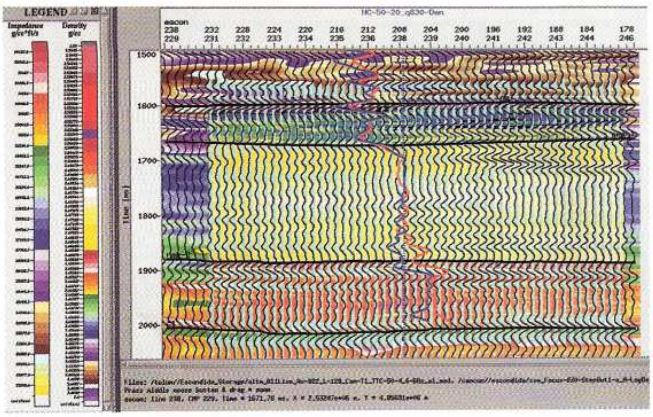

Figure 12. Close-up view of reservoir density estimated in the vicinity of a control well (acoustic impedance and density logs in blue and red, respectively). Acoustic impedances obtained with trace-based inversion are displayed in the background for reference. Black wiggles are the original seismic traces, and cyan wiggles correspond to residual errors yielded by geostatistical inversion.

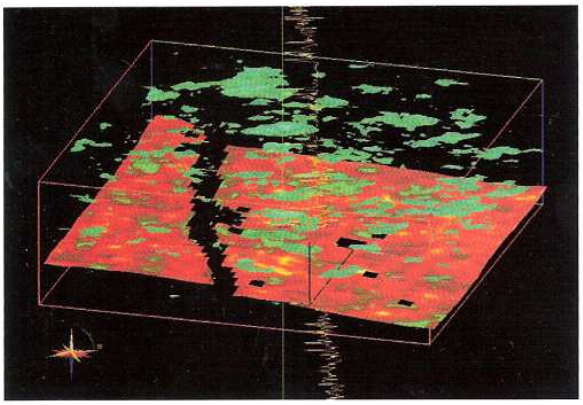

Figure 13. 3-D view of porous sand units estimated with trace-based and geostatistical inversion in the vicinity of a control well. Individual sand units are shown in green. The lower time horizon is displayed here to give an indication of embedding structure.

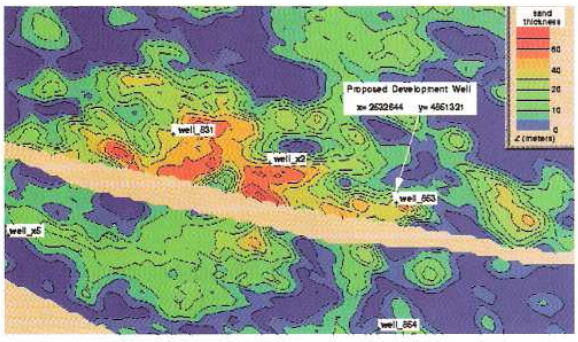

Figure 14. Plan view of total sand thickness estimated between compartments B and C. The well location indicated by the arrow was proposed on the basis of this map and in light of structural trapping and hydrocarbon maturation and migration studies. Purple and red indicate small and large sand thicknesses, respectively.

by trace-based inversion. The geostatistical realizations are further constrained to exactly match the wellbore data at wells. Each couple of independently (stochastically) generated density and lithology samples is then fed to the assumed petrophysical relationship that ties them with a unique AI value. This petrophysical relationship is assumed representative of reservoir behavior within the frequency range of the measurements. Subsequently, AI values are used to simulate the poststack seismic data by convolving them with the same wavelet used with trace-based inversion. Should the simulated data depart significantly from the actual seismic data, both realizations of density and lithology are rejected, and new ones are drawn from their corresponding PDFs. The procedure repeats itself until an appropriate matching criterion is satisfied over the entire seismic cube. At the end of this process we are left with three property cubes: AI, density, and lithology, all related through the assumed underlying petrophysical relationship.

Finding the appropriate distributions of both lithology and density can be computer intensive since in general tens of realizations are needed to properly describe the existing set of solutions (the inversion is, in general, nonunique). We implemented a simulated annealing technique to sample the PDFs to search for a solution that satisfies the data. This proved efficient and can be improved with less CPU-intensive search algorithms such as Metropolis or ad hoc Monte Carlo sampling or by resorting to parallel CPUs.

For simplicity, we considered only three lithologies—shales/tuffs, tight sands, and porous sands. The PDF for lithology was sampled from several well logs and corresponded to 80%, 15%, and 5% flat probabilities assigned to shales/tuffs, tight sands, and porous sands, respectively. A petrophysical relationship was then enforced via a table similar to that shown in Figure 4, one table per vertical compartment. The inversions were performed in time, resampling the wellbore data to 0.5 ms to leave room for resolution improvement in the vertical direction. This can potentially give four times the vertical resolution of seismic data alone. The petrophysical tables were modified to accurately represent the desired vertical resolution. Figure 9 is a sample histogram estimated from wellbore data. Figure 10, on the other hand, shows variograms generated from samples of AI.

A cross-section of density estimated in the vicinity of a test well is shown in Figure 11. The density distribution shown was averaged from 30 stochastic realizations, each satisfying both seismic and wellbore data. For comparison, the same figure shows the AI distribution estimated with trace-based inversion. The difference in vertical resolution between the results is clear. In particular, shaly sand packets estimated in compartment A with trace-based inversion are now visible as thinner sand units with the same lateral trend. In the proximity of the well, the estimated density is superior in vertical resolution to the AI distribution rendered by trace-based inversion. Away from the well, the resolution degrades to finally reflect the same vertical resolution exhibited by the inverted AI. The 30 realizations required approximately 45 hours of CPU time on an SGI Octane (195 MHz) computer. Figure 12 is a composite plot intended to show the estimated density distribution together with the input seismic data (black wiggles) and the corresponding residuals (cyan wiggles). Within the area of interest, the residual wiggles are unbiased and smaller than the seismic wiggles. The density distribution was obtained by enforc-

ing a least-squares matching criterion of 1% between the input and numerically simulated seismic data.

Many computer experiments were performed prior to obtaining the results in Figures 11 and 12. We paid close attention to the influence of variograms, histograms, and petrophysical tables on the final results. Although all are important conditioning parameters, enforcing a fit to the seismic data made the results much less sensitive to a small change in histograms and variograms than standard geostatistical estimation.

One important difference between geostatistical inversion of AI and trace-based inversion is that the former does not need to numerically simulate the low-frequency information. In effect, the low-frequency component of AI data is naturally blended into the geostatistical inversion when estimations (a) honor the well data and (b) exhibit the lateral correlation length implicit in the sampled variograms.

Drilling applications. The trace-based and geostatistical inversion procedures helped improve the way in which hydrocarbon fields are developed in San Jorge Basin. For instance, applying a simple threshold filter on AI and/or density leads to 3-D images of sand units such as Figure 13. These can aid the reservoir engineer in visualizing possibilities for in-fill and guided development drilling, especially in conjunction with structural play. However, given the laterally discontinuous character of the sand units in Cañadón de la Escondida, often the best strategy is to drill vertical wells where total sand thickness is maximum and the embedding geologic structures are favorable. Figure 14, a plan view of the total sand thickness within compartments B and C, was obtained by vertical summation of the thickness corresponding to each of the individual sand units in Figure 13. Similar maps have located new development wells (arrow in Figure 14). The total accumulated production of this well is estimated at three times the average value in Cañadón de la Escondida. To date, all wells proposed with this methodology have successfully corroborated predictions of sand presence. Reservoir engineers can now focus on additional variables controlling production, e.g., oil migration and maturation regimes.

Suggestions for further reading. "Lp-norm deconvolution," by Debeye and Van Riel, *Geophysical Prospecting*, 1990, v. 38, p. 381-403. "Evolution of the San Jorge Basin, Argentina" by Fitzgerald et al., *AAPG Bulletin*, 1990, v. 74, no. 6, p. 879-920. "Geostatistical inversion—A sequential method of stochastic reservoir modelling constrained by seismic data" by Haas and Dubrule, *First Break*, 1994, v. 12, no. 11, p. 561-569. "Geostatistical reservoir characterization constrained by 3D seismic data" by Journel and Huijbregts, 1978, *EAEG Expanded Abstracts*. "Reservoir properties inferred from seismic response in areas with minimal well control: The integration of geology, geophysics, petrophysics, and petroleum engineering in reservoir delineation, description and management" by Loren et al., *Proceedings of the 1st Archie Conference*, 22-25 October 1990. "Inversion of seismic and well log data by best feasible approximation" by Malinverno, *SEG Expanded Abstracts*, 1995, p. 1032-1035. "Estimating porosity from 3D seismic inversion and 3D geostatistics" by Pendrel and Van Riel, *1997 SEG Expanded Abstracts*. "Numerical Recipes in C: The art of scientific computing" by Press et al., second edition, Cambridge University Press, 1992. "Reservoir geophysics," Sheriff, editor, 1992, *SEG Investigations in Geophysics No. 7*. E

Acknowledgments: We express our deepest appreciation to Unidad Económica Las Heras, YPF, and the Gerencia de Exploración Regional Sur, YPF, for their help and continued support of this project.

Corresponding author: C. Torres-Verdín, Dept. of Petroleum and Geosystems Engineering, The University of Texas at Austin, TX 78712, U.S., email: C.Torres-Verdin@pe.utexas.edu